The Behavior of Ions near a Charged Wall−Dependence on Ion Size, Concentration, and Surface Charge.

Jesse J. Howard, John S. Perkyns, and B. Montgomery Pettitt*

Department of Chemistry, University of Houston, Houston, Texas 77204-5003

Received: November 16, 2009; Revised Manuscript Received: March 24, 2010

A renormalization of the 3D-RISM-HNC integral equation is used to study the solvent and ion distributions at neutral and negatively charged planar atomistic surfaces. The charge density of the surfaces ranged from 0.0 to 0.4116 C/m^2, and the modeled electrolyte solutions consist of the salts NaCl, KCl, and CsCl at concentrations of 0.1, 0.25, and 1.0 M in SPC/E water. The results are qualitatively compared to the results from other integral equation methods and simulations for similar models. We find that the 3D-IEs predict an electric multilayer screening behavior in the solvent and ion distributions in contrast to the double layer anticipated from Poisson−Boltzmann theory. It is observed that the cation size has a significant effect on the distributions near the surface up to three solvation layers beyond which the behavior is the same among the different cations. The response of the distributions to the charged surface is described as an increase in ion and solvent density near the wall. The higher concentration solutions screen the electrostatic source more strongly at the wall as expected. The importance of ion−solvent and ion−ion correlations near the surface is shown through three-body correlation functions which are obtainable from the 3D-IEs in this study.

I. Introduction

Structural and thermodynamic studies of water in the vicinity of a planar surface constitute a sizable area of research, considering the amount of chemistry done on a solid support in contact with the liquid phase.[1] The importance of using theoretical methods to study the solid/liquid interface is greater emphasized by the fact that acquiring experimental measurements specific for the region near the interface are often hindered by the relatively small amount of liquid in this region compared to the bulk phase.[2] Much is known about the behavior of aqueous species in the bulk phase from experimental and theoretical studies. However, a surface or wall introduces an inhomogeneity such that the bulk properties are no longer applicable in the solid/liquid interfacial region and must be studied explicitly. In this paper, we present a three-dimensional integral equation (3D-IE) study of the liquid structure and electrostatic properties for pure water and aqueous electrolyte solutions near an atomically modeled planar wall for a range of surface charge densities.

The theoretical methods used to study the solid/liquid interface and predict the behavior of the liquid species in this region have steadily developed in the literature.[1,3,4] The early methods for inhomogeneous salt solutions were based on continuum theory presented by Gouy[5] and Chapman[6] and relied on a continuum Poisson−Boltzmann (PB) approach to study the phenomenon of the electrical double layer (EDL). The electrical double layer is a short-range mean field feature of the wall/fluid interactions and exists due to the response of the ion density distributions. In simulations, the EDL is not usually observed per se but a far more rich and complicated multilayer structure is often seen.[7] The counterions in conjunction with the solvent create a polarization to electrostatically oppose a charged source at short ranges.

The PB and modified PB approach have been extensively applied to systems to characterize an EDL.[8−12] The PB theory gives better results for lower concentration solutions and systems with walls containing a lower surface charge.[4,11,13] The way solvent species are described in the PB methods contains an inherent approximation. The theory does not account for the effects of the finite size of the solution species on the intermolecular correlations. This has been shown to lead to overscreening and charge reversal of the double layer.[14] In PB theory, the effects of the solvent are included only through the dielectric screening constant and the mean-field ionic correlation that is obtained is far too simple compared to simulations. For these reasons, statistical mechanics methods checked by simulations have been developed and applied to study these systems with an overall improvement in the description of the density distributions.[15]

A common element in the development of statistical mechanical theories of liquids has been the Ornstein−Zernike equation and its corresponding closures.[16] The equations form a closed set which are usually solved numerically. The exact form of the equations becomes analytically intractable for most systems, and approximations are used. The use of these approximate OZ based theories to study inhomogeneous systems can be seen in many applications including the reference hypernetted chain (RHNC) theory[17−23] and the anisotropic hypernetted chain equation (AHNC).[24−27] These approximations have been applied to systems composed of solutions of polar fluids and large charged hard spheres where the effects of the curvature are often negligible for a sufficiently large sphere, although not all properties converge to the infinite wall limit. In that regard, recent works on nanospheres in solution have relevance to the work presented here.[28]

Other applications for atomistic models involving the reference interaction site model (RISM) theory[29] have also been used to study the solid/liquid interface.[30] RISM theory is different from one-center "molecular" OZ theories in that the interaction between molecular species is described as a sum of atomic potentials and the correlation functions are computed as orientational averages of the molecular correlation functions. Singlet-RISM (SRISM) theory[31,32] is a symmetry reduced form

10.1021/jp9108865
Published on Web 04/20/2010

of the RISM approach that gives the singlet solvent density distributions for the inhomogeneous system. IEs have also been coupled with singlet densities to describe solid/liquid systems in several guises.[33,34]

All of the previously mentioned theoretical methods are reduced from their intrinsically six-dimensional forms for the full angular dependent pair correlations between arbitrary molecules. The resulting correlation function from the partial (approximate) angular integration depends on a distance parameter from the wall, and there is no trivial extension of these methods to study systems where the wall contains anisotropic reference points. For example, a single particle or molecule on the surface would destroy the planar symmetry. In such systems, a single distance parameter normal to the surface does not reasonably characterize the system.

For these reasons, it seems more appropriate to utilize a theory which retains the angular information related to the wall. Here, we employ a renormalized, HNC variant of the three-dimensional RISM theory[35−39] to study the wall−solvent and wall−ion density distributions which will allow for applications to anisotropic wall−solute systems. The focus here will be to extend the ability of the 3D equations to accurately describe the response of the liquid species to the presence of the wall, such as further testing the EDL phenomenon, and to compare the results to the other theoretical methods mentioned earlier.

The 3D integral equation method used here gives an approximate 3D description of the fluid site (atom) density distributions around a solute model. The 3D-RISM family of methods is an extension of 1D-RISM theory where approximate orientational averaging is done only for the solvent molecules. The 3D integral equations have been used to calculate approximate solvent site density distributions around anisotropic solute species and the corresponding solvation thermodynamics. This has interestingly allowed for the structural stability of the solute configurations or conformations to be analyzed in terms of the solvation contributions to the free energy of the system.[40−45]

These types of detailed structural and thermodynamic studies are also desirable for solutes near a surface to analyze the effect of the surface on the conformational stability of a solute molecule. A different variant of 3D-RISM theory has previously been applied to wall−solvent systems containing pure water.[46−48] An application to aqueous electrolyte solutions has not been previously reported, and we pursue that here.

In this paper, we are using the 3D-IEs to predict the solvent and ion density of aqueous electrolyte solutions and pure water near an atomistic wall which can be charged. Section II contains the details of the IEs, method of renormalization, and other theoretical details used in this study. Section III contains the description of our model and parameters. Section IV contains the results with discussion, and section V contains the conclusions.

II. Theory and Equations

To calculate the 3D solvent and ion site density distributions for our system composed of the wall interacting with the aqueous environment, we start with the approximate 3D-RISM equation[35,36,38] in Fourier space.

$$h_{ua}(\mathbf{k}) = \sum_b c_{ub}(\mathbf{k})(\omega_{ba}(\mathbf{k}) + \rho_b h_{ba}(\mathbf{k})) \qquad (2.1)$$

The 3D-RISM equation before the Fourier transformation contains a convolution integral. The function $h_{ua}(\mathbf{k})$ is the solute−solvent site total correlation function between the solute and solvent site a on a 3D grid, $c_{ua}(\mathbf{k})$ is the 3D solute−solvent site direct correlation function, ρ_b is the particle number density of the solvent sites, $\omega_{ba}(\mathbf{k})$ is the intramolecular correlation function describing the molecular geometry of the solvent, and $h_{ba}(\mathbf{k})$ is the solvent site−site total correlation functions. The subscripts in eq 2.1 denote the solute molecule, u, and the specific solvent sites, a and b. The summation is over all solvent sites. The correlation functions in eq 2.1 are numerically transformed from their direct space representation using Fourier methods.

The intramolecular correlation function, $\omega_{ba}(\mathbf{k})$, is approximated in Fourier space as an angle average

$$\omega_{ba}(\mathbf{k}) = \frac{\sin(|\mathbf{k}|l_{ba})}{|\mathbf{k}|l_{ba}} \qquad (2.2)$$

where $\mathbf{k}$ is the Fourier space vector, $l_{ba} = |\vec{l}_{ba}|$ is the distance between sites b and a on the same species, $\omega_{ba}(\mathbf{k}) = 0$ for sites on different species, and $\omega_{aa}(\mathbf{k}) = 1$.

The solvent site−site total correlation functions, $h_{ba}(\mathbf{k})$, used here are calculated using the dielectrically consistent RISM theory[49,50] and are used in the Fourier space representation of eq 2.1.

The closure relation used in this study is the well-known hypernetted chain (HNC) equation which relates the two unknown functions $c_{ua}(\mathbf{r})$ and $h_{ua}(\mathbf{r})$. The closure is calculated using the direct space representation of the correlation functions from eq 2.1. The HNC equation for the site−site models is defined as

$$c_{ua}(\mathbf{r}) = \exp(-\beta u_{ua}(\mathbf{r}) + t_{ua}(\mathbf{r})) - t_{ua}(\mathbf{r}) - 1 \qquad (2.3)$$

The function $t_{ua}(\mathbf{r}) = h_{ua}(\mathbf{r}) - c_{ua}(\mathbf{r})$ is the indirect correlation function, $u_{ua}(\mathbf{r})$ is the pair interaction potential between the molecular solute and the solvent site a, β is the inverse of the product of the system temperature and Boltzmann's constant, and the indices specify the sites. In the 3D calculations, solvent species are represented on a lattice and distances are calculated from the solute sites to the lattice sites.

The use of the Fourier transform technique is fairly straightforward for model interaction potentials which decay at least as fast as r^{-4}. The Coulomb interaction potential, which is used to describe the electrostatic interactions of the wall and ion sites in this study (shown in eq 3.1), does not decay fast enough, and extra steps must be taken to obtain numerically transformable functions. The functions are usually separated into a long-ranged analytically transformable part and a short-ranged numerically transformable part.[51] The derivation and implementation of this method for the 1D-IEs is described in numerous sources.[52−54] The extension of this method to the grid based 3D-IEs was recently derived and implemented by Perkyns et al.[15]

The decomposition of the potential into long- and short-ranged functions is analogous to the 1D method using the error function; however, the Fourier transform contains a phase factor which arises due to the positions of the charged sites with respect to an arbitrary origin. The Coulomb potential can be split into a short-ranged part and a long-ranged part. The decomposition is not unique, but a useful way to write the long-ranged part for the solute−solvent site Coulomb interaction is

$$\theta^l_{ua}(\mathbf{r}) = \sum_{b\in u} \mathrm{erf}(\alpha|\mathbf{r} - \mathbf{r}^u_b|)\frac{q^v_a q^u_b}{|\mathbf{r} - \mathbf{r}^u_b|} \tag{2.5}$$

where the summation is over all solute sites b (this includes the ion and wall sites in this study), $\mathbf{r}$ is the vector from an arbitrary origin to a grid point, $\mathbf{r}^u_b$ is the vector from solute site b to a grid point, q^v_a is the charge on the solvent site, q^u_b is the charge on the specific solute site, and α is assigned a value of 1.08 for most cases. The definition of the 3D Fourier transform of the long-ranged part on the 3D grid is

$$\theta^l_{ua}(\mathbf{k}) = \int \mathrm{d}\mathbf{r}\, \exp(-i\mathbf{k}\cdot\mathbf{r}) \sum_{b\in u} \mathrm{erf}(\alpha|\mathbf{r} - \mathbf{r}^u_b|)\frac{q^v_a q^u_b}{|\mathbf{r} - \mathbf{r}^u_b|} \tag{2.6}$$

After a change of variables, where $\mathbf{r}' = \mathbf{r} - \mathbf{r}^u_b$, the equation is expressed as

$$\theta^l_{ua}(\mathbf{k}) = \int \mathrm{d}\mathbf{r}' \sum_{b\in u} \exp(-i\mathbf{k}\cdot(\mathbf{r}'+\mathbf{r}^u_b)\, \mathrm{erf}(\alpha|\mathbf{r}'|)\frac{q^v_a q^u_b}{|\mathbf{r}'|} \tag{2.7}$$

and after transforming the variable $\mathbf{r}'$, the Fourier space definition of the long-ranged potential is given simply as

$$\theta^l_{ua}(\mathbf{k}) = \sum_{b\in u} \exp(-i\mathbf{k}\cdot\mathbf{r}^u_b)\frac{q^v_a q^u_b}{|\mathbf{k}|} \exp\left(\frac{-k^2}{4\alpha^2}\right) \tag{2.8}$$

The short-ranged potential is then the difference

$$\theta^s_{ua}(\mathbf{r}) = \beta u_{ua}(\mathbf{r}) - \theta^l_{ua}(\mathbf{r}) \tag{2.9}$$

and the short-ranged, transformable correlation functions are expressed as

$$c^s_{ua}(\mathbf{r}) = c_{ua}(\mathbf{r}) + \theta^l_{ua}(\mathbf{r}) \tag{2.10}$$

$$t^s_{ua}(\mathbf{r}) = t_{ua}(\mathbf{r}) - \theta^l_{ua}(\mathbf{r}) \tag{2.11}$$

The variable $\mathbf{r}$ in eqs 2.10 and 2.11 can be interchanged with the Fourier space variable $\mathbf{k}$ for the same definitions of the short- and long-range functions in Fourier space. Finally, the renormalized HNC closure using the short-ranged functions can be written as

$$c^s_{ua}(\mathbf{r}) = \exp(-\beta u^s_{ua}(\mathbf{r}) + t^s_{ua}(\mathbf{r})) - t^s_{ua}(\mathbf{r}) - 1 \tag{2.12}$$

This decomposition of the correlation functions allows use of numerical Fourier transforms during the solution procedure. Importantly, either the long-range Coulomb potential needs to be resummed in Fourier space as described in ref 53 or the decomposition and reconstruction of the correlation functions (eqs 2.10 and 2.11) must be done at each point in the iterative process where a Fourier transform is performed. This point-grid electrostatic renormalization is used here to avoid supercell "Ewald-like" approximations.[15,39]

TABLE 1: Wall and Solvent Interaction Site Parameters

site	σ (Å)	ε (kJ/mol)	q (e)
C−wall	3.410	0.3598	0.0 → ±0.03
O−water	3.166	0.6505	−0.8476
H−water	0.400	0.1926	0.4238

The probability distributions calculated from the 3D-IEs are functions of three spatial coordinates x, y, and z, with z being the coordinate perpendicular to the surface. To compare correlations with the wall from the 1D theories, we only need average distributions to produce functions of the z coordinate. The 1D distributions are calculated by integrating the x and y coordinates over a region centered on the plate.

$$g(z) = \frac{1}{\Delta x \Delta y}\int g(x, y, z)\, \mathrm{d}x\, \mathrm{d}y \tag{2.13}$$

Once the distribution functions for the solvent and ions are obtained, the potential of mean force (PMF), $w(z)$, can be calculated using

$$w(z) = -\beta^{-1} \ln g(z) \tag{2.14}$$

In addition to calculating the density distributions of the atomic sites of the molecules of the liquid, we also calculate the charge density distributions of the ions and solvent as a function of the distance to the surface using

$$\rho_q(z) = \sum_{\alpha=\pm} \rho_\alpha q_\alpha g_\alpha(z) \tag{2.15}$$

III. Model

Our model system consists of a planar wall in either pure water or an aqueous electrolyte solution with various ion concentrations. The interactions between the wall, ions, and solvent species are represented by the sum of a Lennard-Jones 6−12 interaction potential (LJ) term and a Coulomb electrostatic term (eq 3.1). The total site−site pair interaction potential is expressed as

$$u_{ab}(r) = 4\varepsilon_{ab}\left(\left(\frac{\sigma_{ab}}{r}\right)^{12} - \left(\frac{\sigma_{ab}}{r}\right)^{6}\right) + \frac{q_a q_b}{r} \tag{3.1}$$

where ε and σ are the energy and distance parameters for the well depth and site diameter, respectively, and the indices, a and b, specify the sites of the solute and solvent species. The interaction parameters between different sites are calculated using the Lorentz−Berthelot mixing rules

$$\sigma_{ab} = (\sigma_{aa} + \sigma_{bb})/2 \tag{3.2}$$

$$\varepsilon_{ab} = \sqrt{\varepsilon_{aa}\varepsilon_{bb}} \tag{3.3}$$

The wall is constructed from a planar array of atomic "carbon" interaction sites.[55] The site positions are arranged in accord with the face of a cubic lattice with distances of 1.38 Å between adjacent sites. The wall consists of 21 sites to a side

TABLE 2: Ionic Model Parameters for the Aqueous Electrolyte Solutions

ion	σ (Å)	ε (kJ/mol)	q (e)
Na	2.583	0.5216	1.0
K	3.331	0.5216	1.0
Cs	3.883	0.5216	1.0
Cl	4.401	0.5216	−1.0

for a total of 421 interaction sites measuring 30 Å × 30 Å. The size of the wall was chosen so that a substantial amount of space near the center of the wall was not affected by edge effects and thus more accurately represents the macroscopic case. The charge and LJ parameters for the wall−atom sites and solvent−water sites are given in Table 1.

The parameters for the water sites are from the SPC/E water model. The parameters for the wall−atom sites are taken from previous studies of carbon-like walls[48,56] in the aqueous environment. The water model is described by three interaction sites located at the atomic positions of the oxygen and hydrogen sites. The bond angle is 109.5°, and the oxygen−hydrogen bond distances are 1.0 Å. The number density for the water molecules is taken as 0.03334 at a system temperature of 300 K.

For the aqueous electrolyte solutions, a series of ion parameters are used which resemble NaCl, KCl, and CsCl ionic solutions.[57] The series was chosen to study the effects of the cation size on the ionic density distributions and the effective screening of a charged wall by the counterions. The parameters for the ion models are given in Table 2. The LJ epsilon values, ε, are the same in order to simplify and classify the effects due to ion size and not the interaction potential. Three different concentrations are used for the electrolyte solutions, 0.1, 0.25, and 1.0 M, to study the behavior of the ions at a charged wall. The Na^+ ion diameter is less than that of the solvent−water which could change the balance in structure of counterions between the surface and first hydration layer. The K^+ ion diameter is similar to the O−water diameter, and the closest distance contact peaks will occur near the contact peaks of the oxygen distributions. The Cs^+ ion diameter is larger than the oxygen diameter which will ensure that the first possible counterion contact layer occurs at distances greater than the first peak of the first hydration layer.

The 3D distributions are calculated on a grid of 256^3 points; some calculations are checked for convergence with 512^3 grids. The total space covered measured 60^3 Å^3, which gives a voxel resolution of 0.235^3 Å^3. The wall is placed in the $x-y$ plane in the center of the box. The HNC closure for the solute−solvent correlations is set to $h(z) = -1$ for $z < 0$, i.e., inside the wall. This ensured no liquid species are "behind" the wall. The equations are solved using a modified direct inversion in the iterative subspace (MDIIS) routine[58,59] with a subspace of five vectors, and the 3D Fourier transforms are carried out using the FFTW package.[60] The input isotropic solvent−solvent and ion−solvent correlations are calculated on a grid with a spacing of $\Delta r = 0.004$ Å using dielectrically consistent reference interaction site model (DRISM) theory.[49,50] In order to avoid grid dependent numerical problems from the coarse grid spacing of the 3D grid, the 1D solvent−solvent correlations are best included in the 3D-RISM equations using their Fourier space representation.

IV. Results and Discussion

In the absence of any electrostatic charges, the steric interactions combined with the dispersion forces influence the orientation of the solvent molecules at the surface, leading to a nontrivial electric field at the solid/liquid interface. In order to characterize the further changes in the density distributions due to the inclusion of surface charges, we start this section with the results for a neutral wall in our aqueous solutions. The results for the charged plates follow and are analyzed relative to the distributions calculated from the neutral surface. These results will also be compared to the results from other IE methods (SRISM) and simulations for similar models when available. The equations above are solved for pure water and 0.1, 0.25, and 1 M aqueous electrolyte solutions of NaCl, KCl, and CsCl.

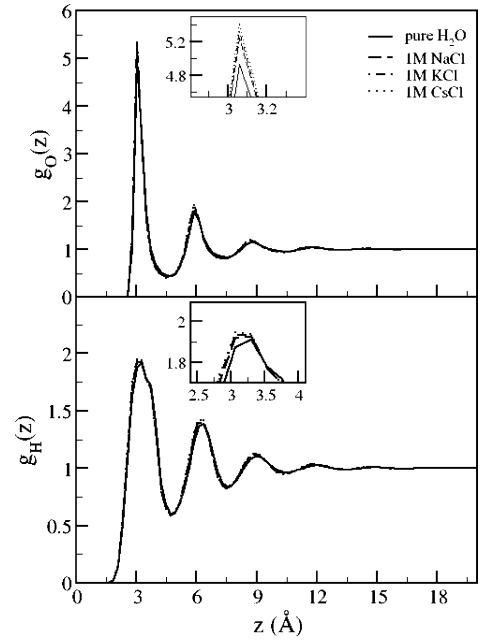

Figure 1. Wall−oxygen (top) and wall−hydrogen (bottom) distributions for a neutral surface in the model 1 M aqueous electrolyte solutions. The four different distributions are for pure water (solid), 1 M NaCl (dashed), 1 M KCl (dot-dashed), and 1 M CsCl (dotted) solutions.

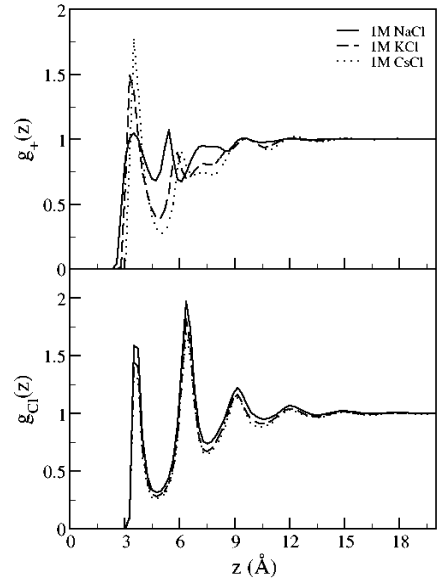

Figure 2. Wall−cation (top) and wall−anion (bottom) distributions for a neutral wall and ionic aqueous solutions for 1 M NaCl (solid), 1 M KCl (dashed), and 1 M CsCl (dotted) solutions.

A. Neutral Wall. The solvent distributions for the water sites $g_O(z)$ and $g_H(z)$ of the pure water and 1 M aqueous electrolyte solutions near the wall are shown in Figure 1. The first peak or contact peak of $g_O(z)$ for pure water is at a height of 5.0 which

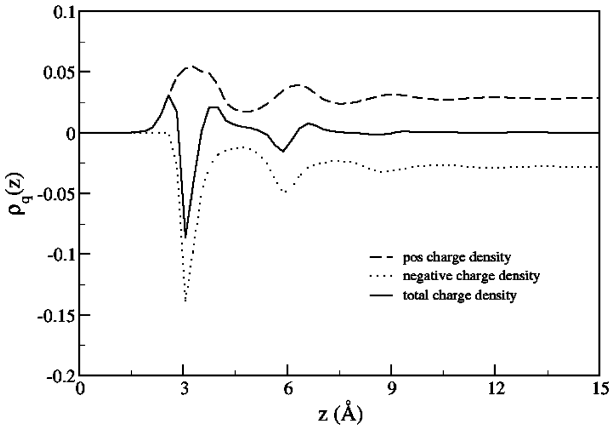

Figure 3. Total charge density ($-e/Å^3$) for pure water at a neutral surface.

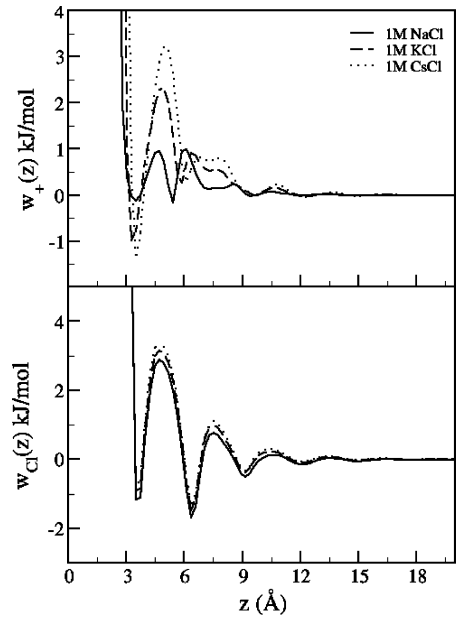

Figure 4. PMF for the cations in electrolyte solutions as a function of distance from a neutral surface for 1 M NaCl (solid), 1 M KCl (dashed), and 1 M CsCl (dotted) solutions.

appears to be nearly identical to the results reported by SRISM theory.[31] Although slightly different wall interaction parameters are used in this study compared to the SRISM study, the structural similarities of the solvent distributions between the IE theories near the neutral wall are most likely due to steric interactions between the water sites and neutral wall. The 3D-IEs and the SRISM both overestimate this peak compared to the simulation results.[31] The overall structure of the solvent is best described as a series of decreasing layers with a distance of ~2.9 Å between adjacent layers. These layers decay to the bulk density after about four layers or ~12 Å in this system.

The cation and anion distributions with the neutral wall for the 1 M aqueous electrolyte solutions are shown in Figure 2. The ion parameters, defined in section III, show that the only differences among the cations are the physical diameters of their ionic spheres; however, according to Figure 2, this can result in significant differences in the ion distributions for up to three solvation layers from the wall interface. In a continuum solvent model theory, the behavior of the different sized cations shows less pronounced changes.[12] However, using the site−site integral equations which account for the excluded volume of the solvent, the structure of the Na^+ cation distributions is noticeably different from the K^+ and Cs^+ distributions. The first two peaks in the Na^+ distributions are roughly equal in height and are just slightly above the bulk value of 1.0. The K^+ and Cs^+ distributions show a stronger contact peak than the Na^+ distributions with a height of 1.5 and 1.8, respectively. The increase in height of the contact peak as the ion size increases has been observed before in other studies which account for the excluded volume of the ion species and can be attributed to a decrease in accessible volume for the larger ions which leads to decreased entropy for the system and thus a more ordered system.[61−63] The height of the second peak in the K^+ and Cs^+ distributions is lower than the first peak and less than the second peak of the Na^+ distribution function.

In the SRISM results,[31] where the cation in that study is most similar to the K^+ ion in this study, a contact peak with a height of 1.5 is observed which is identical to the peak height of the K^+ distributions in this study. However, the second peak in the SRISM results was much greater than the bulk density with a height of ~1.7, while the second peak in this study for the K^+ distributions was less than the bulk value with a height of 0.88. The SRISM and our 3D-IE results are both in contrast to a set of simulation results where the ions were completely displaced from the first wall solvation layer.[31] The IE methods found the presence of ions in the first solvation layer next to the uncharged wall to be a prevalent feature even with over 50 times less number density than water.

The diameters of the three cations Na^+, K^+, and Cs^+ differ from the water−oxygen diameter by factors of 0.83, 1.05, and 1.23, respectively. In Figure 2, the first (contact) peak in all of the cation distributions lies within the first solvation layer. It was mentioned earlier that dispersion and packing forces alone are enough to influence the orientation of the solvent water molecules at the wall interface leading to nontrivial electrostatic layers in the solvent—in this case correlated with the average water dipole orientation at the surface. From a purely electrostatic argument, ions favor a polarized environment. The charge density distribution for pure water is shown in Figure 3 in order to consider the electrostatic environment at a distance from the surface. The charge density distributions for the aqueous electrolyte solutions were not included only because the differences in the plots are minimal.

Comparing the location of the maximum height in the contact peaks in Figure 2 and the distance of closest approach of the ions to the wall interface shows some unique behavior in the Na^+ distribution function compared to the other cations used here. The contact peak of the Na^+ distributions occurs at a longer distance than would be expected, and the peak width is broadened. The reason for this behavior can be explained from the charge distribution of the solvent sites and the desolvation penalty of the smaller Na^+ ions. As can be seen by comparing Figures 2 and 3, the Na^+−wall peak is pushed back to a more negative field environment. If the peak was not pushed to larger distances and broadened, a greater portion of the Na^+ site distributions would lie in the unfavorable positively polarized environment. The first peak of the K^+ and Cs^+ distributions occurs in this more negatively charged environment due to their steric diameters. This argument in conjunction with the entropic arguments discussed earlier[28,61,63,64] give a consistent picture for the behavior of the cation distributions and illustrates the importance of having explicit models for the solvent species.

The potentials of mean force (PMF) for the cations with the neutral wall in the 1 M solutions are shown in Figure 4. The PMF for the cations K^+ and Cs^+ show an energetically favorable

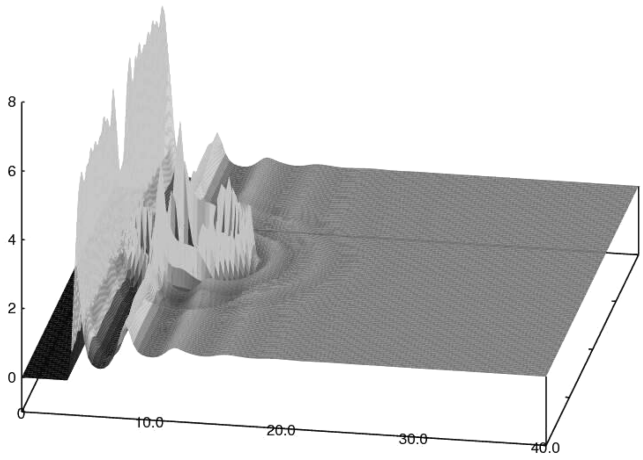

Figure 5. Two-dimensional cut of the density of the water oxygen sites from the wall when a single sodium cation is held 7.0 Å from the wall (distance is from center of wall atoms to ion center).

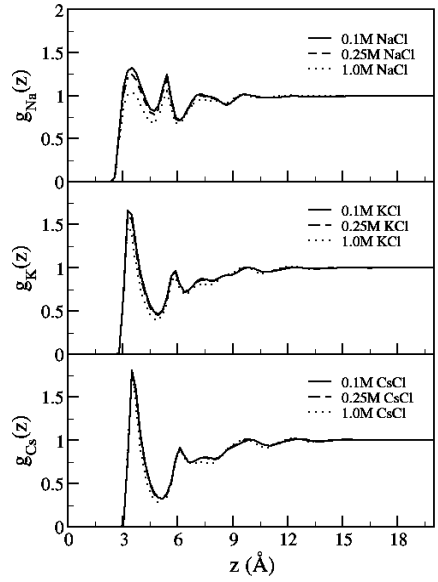

Figure 6. Wall−Na^+ (top), wall−K^+ (middle), and wall−Cs^+ (bottom) distributions for three different salt concentrations near an uncharged wall.

absorption at the contact configuration. These contact configurations are separated from the bulk environment by large activation barriers of 2.3 and 3.2 kJ/mol, respectively, before tailing off to the bulk value near three solvation layers. The PMF for the Na^+ ion does not show any significant preference to be near the wall versus in the bulk. It only shows two small barriers before the bulk phase. The PMF for the Cl^- anions for the same 1 M solutions are also shown in Figure 4. For these more concentrated 1 M aqueous electrolyte solutions, there are only slight quantitative variations in the maxima and minima of the PMF for the anions. It can be deduced from Figures 1 and 4 that an increase in the water−oxygen site density distributions is correlated with a slight decrease in the contact peak of the Cl^- anion distributions.

In Figure 5, we show a two-dimensional cut of the density of the water oxygen sites from the wall when a single sodium cation is held 7.0 Å from the wall (distance is from center of wall atoms to ion center). The density waves caused by both the wall and the ion interfere. The effects are not a trivial superposition of the two sources of anisotropy but are the self-consistent result of the consequences of having both.

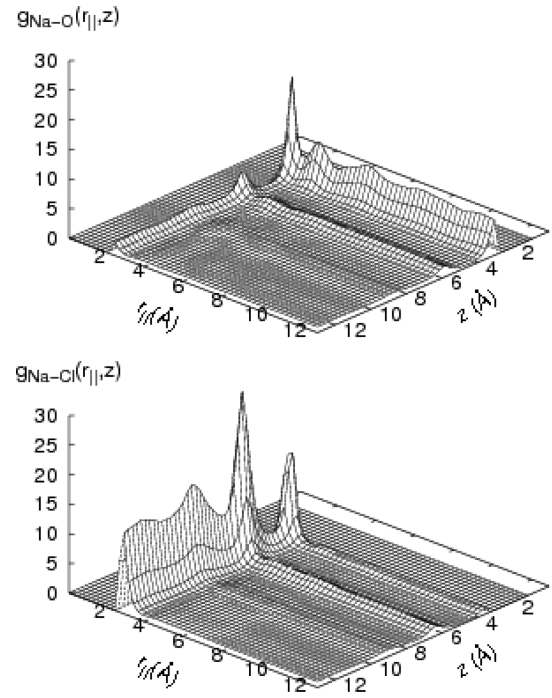

Figure 7. A cut through the three-body distributions for Na^+ with the water oxygen (top) and chloride (bottom) parallel to the plate, $r_{||}$ (Å), and as a function of distance from the plate, z (Å).

We find there is not much difference among the average wall−solvent site (O,H) distribution functions for the different aqueous ionic solutions (see Figure 1); however, the presence of the electrolytes seems to cause a slight increase in the heights of the contact peak heights of $g_O(z)$ and $g_H(z)$. The value of the wall contact peak height of $g_O(z)$ increases from 5.0 for pure water to 5.3−5.4 for the different electrolyte solutions. The increase in the $g_H(z)$ peak heights for the electrolyte solutions is less. Although subtle, this seems to suggest increased ordering of the solvent molecules in addition to the increase in order of the ions (discussed earlier) near the wall due to the presence of the ions and their size. We see that the presence of the ions produces a contraction of the water distributions and leads to a somewhat greater packing density of the water molecules at the surface. The change in packing density in aqueous solutions is an experimentally observed phenomenon.[65,66]

Figure 6 shows the ion concentration dependence of the distribution functions for the cation species. The largest difference is observed in the Na^+ distribution functions at the various concentrations. In general, as the concentration is decreased, the height of the contact peak increases, which follows the well-known trends of primitive ion models.[67,68] In Figure 6, it can be seen that in the lower concentration limit the interaction of the Na^+ cation with the wall becomes more favorable than at the higher concentrations. In other words, as the concentration decreases, the effective interaction between the Na^+ cation and the wall becomes more favorable. This is an example of the counterbalancing effects that give rise to the screening correlations between the species.

In order to show the importance of ion−ion and ion−solvent correlations near the wall, we have included cuts through the three-body distribution functions for the wall−ion−water distribution in 1 M NaCl solution. The three-body correlations contain important information not available from two-body functions and may be calculated from the current methods as conditional cuts. The three-body distributions for species including the wall, water sites, chloride, or sodium ion sites

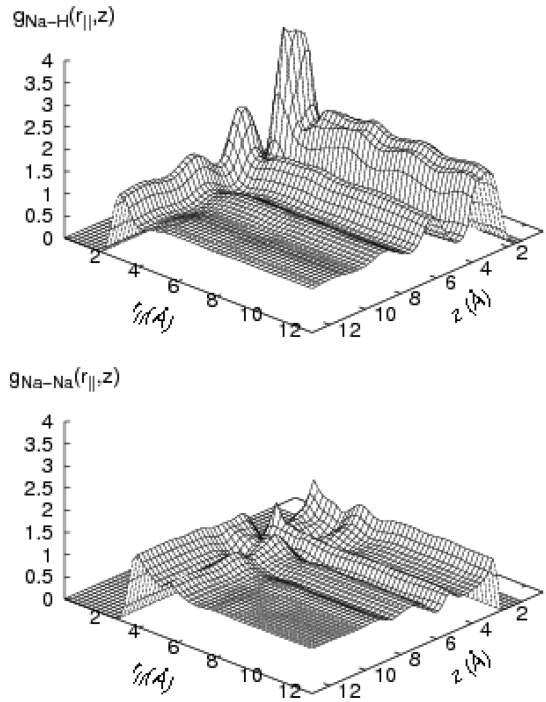

Figure 8. A cut through the three-body distributions for Na^+ with water hydrogen (top) and Na^+ (bottom) parallel to the plate, $r_{||}$ (Å), and as a function of distance from the plate, z (Å). Note the change in scale from the previous figure.

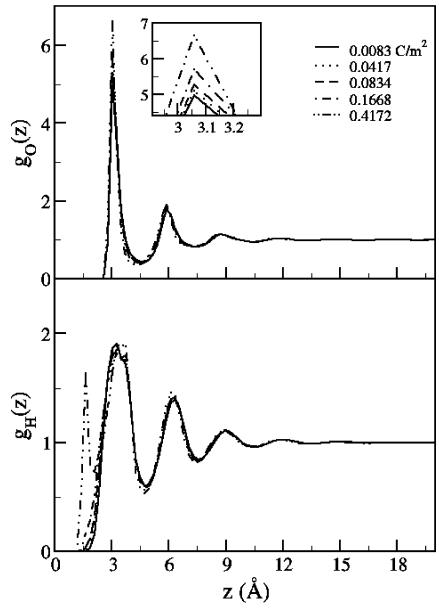

Figure 9. Wall−oxygen (top) and wall−hydrogen (bottom) site distributions for pure water near the charged walls for five different surface charges. The inset shows variations in the peak of the wall−oxygen distributions.

are shown in Figures 7 and 8. As a Na^+ ion approaches the wall, the response in the solvent and ion distributions not only depends on the distance from the ion but also the distance from the surface which can be seen in Figure 7 or 8 for all cases. In the Na^+ ion−solvent−wall distributions, the overlap of the effects from the surface and Na^+ ion again are not a superposition of the two-body correlations. For the Na^+−Na^+ distributions, the response is similar with large changes in the distributions as the ion passes through the high and low solvent density regions. We note that the Na−O and Na−Cl correlations shown in Figure 7 have considerably larger features than the

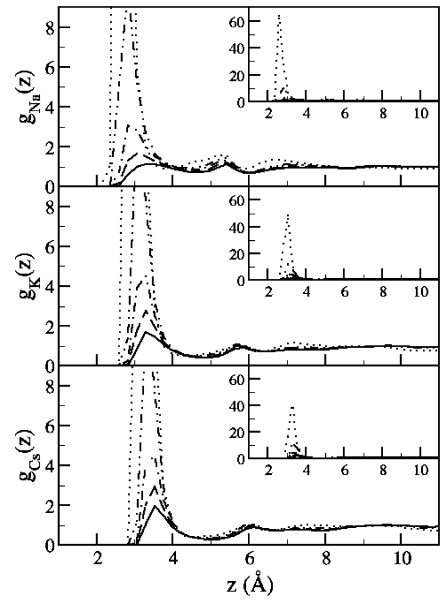

Figure 10. Wall−cation distributions for the 1 M aqueous electrolyte solutions of NaCl, KCl, and CsCl for five different surface charge densities. The different surface charge models are represented by the solid line (0.0083 C/m^2), the dashed line (0.0417 C/m^2), the dash-dotted line (0.0834 C/m^2), the dash-double-dotted line (0.1668 C/m^2), and the dotted line (0.4172 C/m^2). The inset has a reduced scale to show the entire range.

Na−H and Na−Na correlations in Figure 8. Few other techniques are capable of calculating this information in a computationally tractable manner.[34]

B. A Negatively Charged Wall. We now turn to the effects of a charged wall. The wall−solvent site distributions for water near the negatively charged walls are shown in Figure 9 for a range of surface charge densities. Compared to $g_H(z)$, the behavior of $g_O(z)$ is less sensitive to the magnitude of the surface charge with a gradual increase in the height of the contact peak with increasing surface charge. We expect $g_H(z)$ to be dominated by orientation preferences versus $g_O(z)$ which has strong packing requirements. The peak height for $g_O(z)$ increases from 5.0 for the uncharged surface to 6.6 for the highest charged surface studied here. Although slightly different surface charge densities were used in this study compared to a previous SRISM study, the results for the response of the contact peaks in the oxygen site distributions are in general agreement.[32] The wall−solvent hydrogen site distributions show more qualitative shape changes to the increase in surface charge especially at the highest charge. There is an increase in the site distributions at the solid/liquid interface followed by the advent of a new peak in the wall−hydrogen site distributions at a distance of ∼1.5 Å for the highest charged surface (0.4172 C/m^2) which is also seen in the SRISM results.[32] This observation is consistent with a greater distribution of water molecules orientated with their dipoles toward the charged surface compared to the neutral surface.

Figure 10 contains the wall−cation (Na^+, K^+, Cs^+) distributions over the full range of surface charged densities in this study. As the charge density increases, the relative response of the ion distributions is much greater than the response seen in the water distributions. There is a steady increase in the magnitude of the cation distributions as the surface charge is increased in the first two ionic layers with the response in the first ionic layer being much greater than that in the second ionic layer. This shows the anticipated response of the ions at the charged surface and the ability of the current theory to account

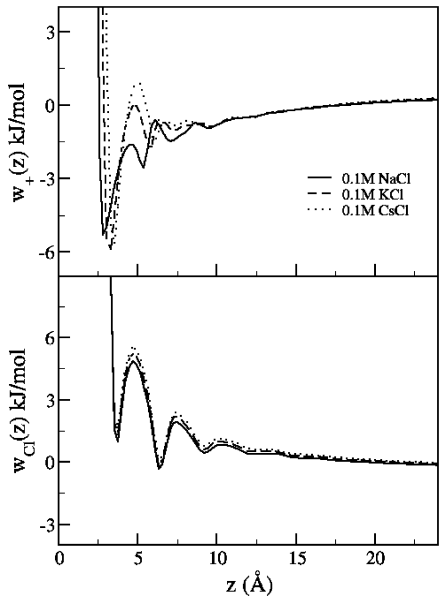

Figure 11. PMF for the different cations (top) and chlorine ions (bottom) as a function of distance from the wall with a surface charge density of 0.0834 C/m^2 for 1 M NaCl (solid), 1 M KCl (dashed), and 1 M CsCl (dotted) solutions.

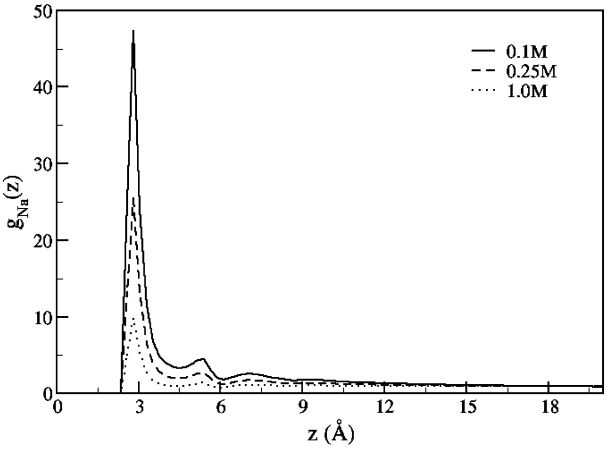

Figure 12. Wall−Na^+ ion site distributions for different concentrations of NaCl electrolyte solution near the surface with a surface charge density of 0.1669 C/m^2.

for the effective screening of the surface charge by an increased presence of counterions at the solid/liquid interface.

An interesting feature of the cation distributions as the surface charge increases is the reversal of the order of the peak heights among the cations. As the surface becomes more negatively charged, the response in the height of the contact peak for the smaller cations is greater than that for the larger cations. The peak height of 68 for the Na^+ distribution at the wall with a charge density of 0.4172 C/m makes it the highest peak followed by the peak height of the K^+ distribution and finally the peak of the Cs^+ distributions. This order is opposite to that seen for the neutral wall−cation distribution peak heights and is in part presumable due to the dominance of the surface field strength of the smaller ions compared to the desolvation penalty. The different effective neutralizing strengths between different sized ions have been previously reported using IE theories.[61,63] In those studies, it was shown that size asymmetry between the co- and counterions is able to enhance the absorption of counterions at the surface as the co-ion size increases or size asymmetry increases. The ion size and the corresponding entropic effects

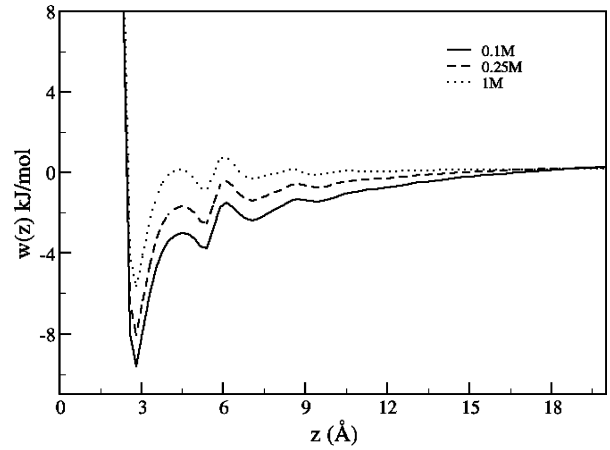

Figure 13. PMF for the Na^+−wall interaction at different concentrations of the NaCl electrolyte near the surface with a surface charge density of 0.1669 C/m^2.

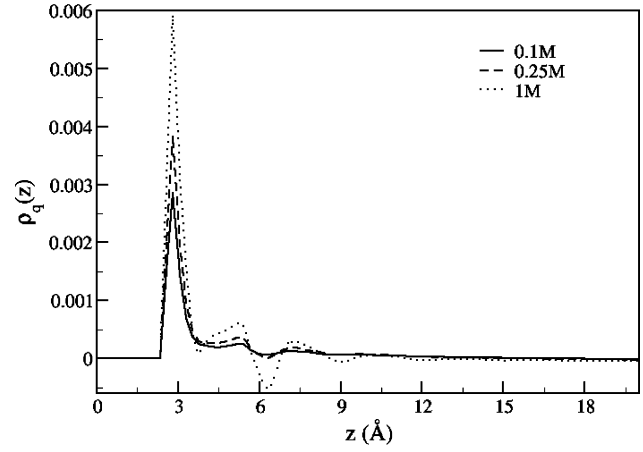

Figure 14. Charge density profile for the Na and Cl ions according to eq 2.15 at different concentrations near the surface with a surface charge density of 0.1669 C/m^2.

have also been implicated in the determination of the effective pair potential between ions and solvent species.[64]

The qualitative behavior of these peaks is similar to the SRISM results; however, the first peak in the cation distributions from the 3D-IE results here are about a factor of 3 less than the SRISM results and lie somewhere between the SRISM/HNC and SRISM/KH results, where the latter is known to severely underestimate correlation effects.[15,69] The KH closure contains a partially linearized form of the HNC, and it is routinely observed that the KH closure underestimates the strength of the contact peaks, whereas the HNC closure can overestimate the strength of the contact peak.[15,69] A notable difference between the models in the two studies is that the surface is smooth in the SRISM study while the surface is textured in the present study due to the atomic surface sites, but this should be a small effect for many properties.

The short-range behavior of the cation distributions was found to be highly dependent on the ion diameters. To study the long-range behavior of the wall−ion interactions, we calculated the PMF for the three cations in 0.1 M electrolyte solutions for the wall with a surface charge density of 0.0834 C/m^2 (Figure 11). The 0.1 M case was chosen because the higher concentration solutions are able to more effectively screen the surface charge and thus reduce the effective potential of the wall seen by the solvent at longer ranges. The short-range behavior unique to each of the cations can be seen up to about three solvation layers

after which the cations all show the same long-range behavior which is predicted by mean-field theories; the long-ranged behavior eventually reaches the expected dielectric continuum result. This is also shown in the PMF for the Cl^- anions corresponding to the same systems (Figure 11). This long-ranged behavior is also found in the results from RHNC theory for aqueous electrolyte solutions near a charged surface[17] as expected.

The electrolyte solution effectively screens the charged surface through a multilayering effect which is much more complex than a simple double-layer picture and has implications for the design of electrolytic cells and other electrode−solvent systems. The wall−Na^+ cation distributions for ion concentrations of 0.1, 0.25, and 1.0 M are shown in Figure 12 where the charge density on the wall is 0.1669 C/m^2. The contact peak height (47) for the 0.1 M solution is much higher than the contact peak height (10) for the 1.0 M solution. The significance of this observation is that relative to the bulk concentration there is a higher ratio of ions at the solid/liquid interface for the lower concentration solutions. However, the bulk density of the lower concentration solutions is not high enough to contribute enough counterions to screen the charged surface as effectively as the higher concentration solutions. The greater effective interaction of the higher concentration solutions can be more easily seen in the PMF for the wall−Na^+ interactions (Figure 13) where a longer-ranged behavior is evident in the low concentration solution but is screened in the higher concentration solutions.[70]

The total charge density profiles due to the ions for these same systems are shown in Figure 14. The higher concentration solution results in a larger presence of counterions at the surface which reduces the effective potential of the surface. There also seems to be a larger role of the electrolytes in the second and third solvation layers between 4 and 9 Å which might suggest that screening in the second and third solvation layers (multilayer effect) is also important in the longer-ranged behavior of the wall−ion interactions.

V. Conclusion

In this paper, a renormalization of a 3D-RISM HNC integral equation was used to study the behavior of ions near neutral and negatively charged surfaces in water. We used point-grid electrostatic renormalization to avoid supercell "Ewald-like" approximations.[15,39,69] The wall was constructed from a planar array of atomic sites with graphite-like parameters and a surface charge density ranging from 0.0 to 0.44719 C/m^2. Three different aqueous solutions containing the salts NaCl, KCl, or CsCl at concentrations of 0.1, 0.25, and 1.0 M were considered for the electrolytic solutions. We found utility in considering both the various anisotropic two-body as well as conditional three-body density distributions.

An exact comparison to other IE studies was not possible because no other current theories have incorporated an atomistic model of a wall. However, the results between the current method and SRISM theory were compared qualitatively. It was found that the present results for the neutral and negatively charged surface were almost always in good agreement with the results from SRISM theory. The exception was for the magnitude of the contact peaks in the wall−ion density distributions for the charged wall case. The SRISM theory has previously been compared to simulation results and, except for the ions in the first solvation layer, was in overall agreement.[31,32]

It was found that the present method is able to qualitatively describe the multilayer screening of the Coulomb potential at the wall seen by the fluid. This was studied with different concentration solutions, and it was found that correlations among screening counterions at high concentrations were able to more effectively neutralize a charged surface. The lower concentration solutions were less able to screen the charged surface, and the effects of this were evident in the long-ranged behavior of the PMF for the lower concentration solutions. The reorientation of the polar solvent molecules as the surface charge increased was also seen by the dipole moments directed more toward the surface, as expected from simulation.[71]

We found that different sized ions behave differently in the first few solvation layers. This is not something anticipated from mean-field results like PB theory. We attributed this to the charge density of the sites, the desolvation penalty of the ions near the wall, and entropic effects causing increased ordering. Cations prefer a negatively charged environment, but that is in competition with packing and the correlations of water. A shift in the cation density distributions was observed to coincide with the alternating positive and negative charged layers due to the distribution of the solvent sites at the surface. The effect is that the contact peak for the cations gets reduced when this peak occurs in the positively charged regions. This illustrates the importance of using a full molecular description for the solvent.

This extension to inhomogeneous systems can realistically model an atomistic surface in solvent with local inhomogeneities. The theory will thus allow for application to more interesting surface chemistries in aqueous electrolyte solutions. This work will hopefully serve as a foundation for future contributions on the nature of the liquid/solid interface.

Acknowledgment. This work was supported in part by the National Institutes of Health (GM066813), the Robert A. Welch Foundation (E-1028), and a training fellowship to J.J.H. from the Keck Center for Computational and Structural Biology of the Gulf Coast Consortia (NLM Grant No. 5T15LM07093). We note refs 28 and 64 appeared after our submission and are related to ions near nanospheres which may be compared to the work presented here.

References and Notes

(1) Henderson, M. A. *Surf. Sci. Rep.* **2002**, *46*, 1.
(2) Huisman, W. J.; Peters, J. F.; Derks, J. W.; Ficke, H. G.; Abernathy, D. L.; van der Veen, J. F. *Rev. Sci. Instrum.* **1997**, *68*, 4169.
(3) Blum, L.; Henderson, D. *Fundamentals of Inhomogeneous Fluids*; Marcel Dekker, Inc.: New York, 1992.
(4) Blum, L. *Adv. Chem. Phys.* **1990**, *78*, 171.
(5) Gouy, *J. Phys.* **1910**, *9*, 457.
(6) Chapman, D. L. *Philos. Mag.* **1913**, *25*, 475.
(7) Wong, K.-Y.; Pettitt, B. M. *Biopolymers* **2004**, *73*, 570.
(8) Woelki, S.; Kohler, H. H. *Chem. Phys.* **2000**, *261*, 421.
(9) Woelki, S.; Kohler, H. H. *Chem. Phys.* **2000**, *261*, 411.
(10) Woelki, S.; Kohler, H.-H. *Chem. Phys.* **2004**, *306*, 209.
(11) Attard, P. *Adv. Chem. Phys.* **1996**, *92*, 1.
(12) Torrie, G. M.; Valleau, J. P. *J. Phys. Chem.* **1982**, *86*, 3251.
(13) Carnie, S. L.; Torrie, G. M. *Adv. Chem. Phys.* **1984**, *56*, 141.
(14) Attard, P. *J. Phys. Chem.* **1995**, *99*, 14174.
(15) Perkyns, J.; Lynch, G.; Howard, J. J.; Pettitt, B. M. *J. Chem. Phys.* **2010**, *132*, 064106:1.
(16) Hansen, J. P.; McDonald, I. R. *Theory of Simple Liquids*; Academic Press: San Diego, CA, 1986.
(17) Torrie, G. M.; Valleau, J. P. *J. Phys. Chem.* **1982**, *86*, 3251.
(18) Dong, W.; Rosinberg, M. L.; Perera, A.; Patey, G. N. *J. Chem. Phys.* **1988**, *89*, 4994.
(19) Berard, D. R.; Kinoshita, M.; Cann, N. M.; Patey, G. N. *J. Chem. Phys.* **1997**, *107*, 4719.
(20) Berard, D. R.; Patey, G. N. *J. Chem. Phys.* **1991**, *95*, 5281.
(21) Wei, D.; Patey, G. N.; Torrie, G. M. *J. Phys. Chem.* **1990**, *94*, 4260.
(22) Wei, D.; Torrie, G. M.; Patey, G. N. *J. Chem. Phys.* **1993**, *99*, 3990.
(23) Berard, D. R.; Patey, G. N. *J. Chem. Phys.* **1992**, *97*, 4372.

(24) Wernersson, E.; Kjellander, R. *J. Chem. Phys.* **2006**, *125*, 154702/1.
(25) Kjellander, R.; Aakesson, T.; Joensson, B.; Marcelja, S. *J. Chem. Phys.* **1992**, *97*, 1424.
(26) Kjellander, R. *J. Chem. Phys.* **1988**, *88*, 7129.
(27) Kjellander, R.; Marcelja, S. *J. Chem. Phys.* **1988**, *88*, 7138.
(28) Zhang, D.; Gonzalez-Mozuelos, P.; Olvera de la Cruz, M. *J. Phys. Chem. C* **2010**, *114*, 3754.
(29) Andersen, H. C.; Chandler, D. *J. Chem. Phys.* **1972**, *57*, 1918.
(30) Akiyama, R.; Hirata, F. *J. Chem. Phys.* **1998**, *108*, 4904.
(31) Woelki, S.; Kohler, H.-H.; Krienke, H. *J. Phys. Chem. B* **2007**, *111*, 13386.
(32) Woelki, S.; Kohler, H.-H.; Krienke, H. *J. Phys. Chem. B* **2008**, *112*, 3365.
(33) Chen, Z. M.; Karim, O. A.; Pettitt, B. M. *J. Chem. Phys.* **1988**, *89*, 1042.
(34) Chen, Z.-M.; Pettitt, B. M. *Phys. Rev. B* **1990**, *42*, 8173.
(35) Beglov, D.; Roux, B. *J. Chem. Phys.* **1995**, *103*, 360.
(36) Ikeguchi, M.; Doi, J. *J. Chem. Phys.* **1995**, *103*, 5011.
(37) Beglov, D.; Roux, B. *J. Chem. Phys.* **1996**, *104*, 8678.
(38) Beglov, D.; Roux, B. *J. Phys. Chem. B* **1997**, *101*, 7821.
(39) Kovalenko, A.; Hirata, F. *Chem. Phys. Lett.* **1998**, *290*, 237.
(40) Kinoshita, M.; Okamoto, Y.; Hirata, F. *J. Mol. Liq.* **2001**, *90*, 195.
(41) Kovalenko, A.; Hirata, F. *J. Phys. Chem. B* **1999**, *103*, 7942.
(42) Imai, T.; Kinoshita, M.; Hirata, F. *Bull. Chem. Soc. Jpn.* **2000**, *73*, 1113.
(43) Kovalenko, A.; Hirata, F. *J. Chem. Phys.* **2000**, *113*, 2793.
(44) Imai, T.; Harano, Y.; Kinoshita, M.; Kovalenko, A.; Hirata, F. *J. Chem. Phys.* **2006**, *125*, 024911/1.
(45) Imai, T.; Harano, Y.; Kinoshita, M.; Kovalenko, A.; Hirata, F. *J. Chem. Phys.* **2007**, *126*, 225102/1.
(46) Kovalenko, A.; Hirata, F. *J. Chem. Phys.* **1999**, *110*, 10095.
(47) Kovalenko, A.; Hirata, F. *J. Mol. Liq.* **2001**, *90*, 215.
(48) Howard, J. J.; Perkyns, J. S.; Choudhury, N.; Pettitt, B. M. *J. Chem. Theory Comput.* **2008**, *4*, 1928.
(49) Perkyns, J.; Pettitt, B. M. *J. Chem. Phys.* **1992**, *97*, 7656.
(50) Perkyns, J.; Pettitt, B. M. *Chem. Phys. Lett.* **1992**, *190*, 626.
(51) Allnatt, A. R. *Mol. Phys.* **1964**, *8*, 533.
(52) Hirata, F.; Rossky, P. J. *Chem. Phys. Lett.* **1981**, *83*, 329.
(53) Hirata, F.; Pettitt, B. M.; Rossky, P. J. *J. Chem. Phys.* **1982**, *77*, 509.
(54) Ng, K.-C. *J. Chem. Phys.* **1974**, *61*, 2680.
(55) Cornell, D. W.; Cornell, W. D.; Cieplak, P.; Bayly, C. I.; Gould, I. R.; Merz, K. M.; Ferguson, D. M.; Spellmeyer, D. C.; Fox, T.; Caldwell, J. W.; Kollman, P. A. *J. Am. Chem. Soc.* **1995**, *117*, 5179.
(56) Choudhury, N.; Pettitt, B. M. *J. Am. Chem. Soc.* **2005**, *127*, 3556.
(57) Lynden-Bell, R. M.; Rasaiah, J. C. *J. Chem. Phys.* **1997**, *107*, 1981.
(58) Hamilton, T. P.; Pulay, P. *J. Chem. Phys.* **1986**, *84*, 5728.
(59) Kovalenko, A.; Ten-No, S.; Hirata, F. *J. Comput. Chem.* **1999**, *20*, 928.
(60) Frigo, M.; Johnson, S. G. *Proc. IEEE* **2005**, *93*, 216.
(61) Guerrero-Garcia, G. I.; Gonzalez-Tovar, E.; Chavez-Paez, M. *Phys. Rev. E: Stat., Nonlinear, Soft Matter Phys.* **2009**, *80*, 021501/1.
(62) Messina, R.; Gonzalez-Tovar, E.; Lozada-Cassou, M.; Holm, C. *Europhys. Lett.* **2002**, *60*, 383.
(63) Guerrero-Garcia, G. I.; Gonzalez-Tovar, E.; Lozada-Cassou, M.; Guevara-Rodriguez, F. d. J. *J. Chem. Phys.* **2005**, *123*, 034703/1.
(64) Kung, W.; Gonzalez-Mozuelos, P.; Olvera de la Cruz, M. *Soft Matter* **2010**, *6*, 331.
(65) Stewart, G. W. *J. Chem. Phys.* **1939**, *7*, 869.
(66) Dougherty, R. C. *J. Phys. Chem. B* **2001**, *105*, 4514.
(67) Abbas, Z.; Ahlberg, E.; Nordholm, S. *J. Phys. Chem. B* **2009**, *113*, 5905.
(68) Carley, D. D. *J. Chem. Phys.* **1967**, *46*, 3783.
(69) Perkyns, J.; Lynch, G.; Howard, J. J.; Pettitt, B. M. *J. Chem. Phys.* **2009**, *132*.
(70) Gonzalez-Mozuelos, P. *J. Phys. Chem. B* **2006**, *110*, 22702.
(71) Schweighofer, K. J.; Xia, X.; Berkowitz, M. L. *Langmuir* **1996**, *12*, 3747.

JP9108865